Left-Right Asymmetry and Kinesin Superfamily Protein KIF3A: New Insights in Determination of Laterality and Mesoderm Induction by *kif3A*$^{-/-}$ Mice Analysis

Sen Takeda, Yoshiaki Yonekawa, Yosuke Tanaka, Yasushi Okada, Shigenori Nonaka, and Nobutaka Hirokawa

Department of Cell Biology and Anatomy, University of Tokyo, Graduate School of Medicine, 7-3-1, Hongo, Bunkyo-ku, Tokyo 113-0033 Japan

Abstract. KIF3A is a classical member of the kinesin superfamily proteins (KIFs), ubiquitously expressed although predominantly in neural tissues, and which forms a heterotrimeric KIF3 complex with KIF3B or KIF3C and an associated protein, KAP3. To elucidate the function of the *kif3A* gene in vivo, we made *kif3A* knockout mice. *kif3A*$^{-/-}$ embryos displayed severe developmental abnormalities characterized by neural tube degeneration and mesodermal and caudal dysgenesis and died during the midgestational period at ~10.5 dpc (days post coitum), possibly resulting from cardiovascular insufficiency. Whole mount in situ hybridization of *Pax6* revealed a normal pattern while staining by *sonic hedgehog* (*shh*) and *Brachyury* (*T*) exhibited abnormal patterns in the anterior-posterior (A-P) direction at both mesencephalic and thoracic levels. These results suggest that KIF3A might be involved in mesodermal patterning and in turn neurogenesis.

Furthermore, homozygotes for *kif3A* showed randomization of laterality in heart looping. In contrast to wild-type embryos where almost all have a D-loop heart (situs solitas), ~40% of homozygous embryos exhibited cardiac L-loops (situs inversus). Moreover, their pericardial space was filled with effusion resulting from/in circulatory insufficiency. Scanning electron microscopy (SEM) and video-enhanced contrast DIC and fluorescent images (VEC-DIC/FL) microscopy revealed the absence of motile monocilia on mutant nodal pit cells, which could not generate leftward nodal flow of extraembryonic fluid and are considered to be responsible for initial determination of the left-right (L-R) asymmetry. These results collectively suggest the important role of the KIF3A protein in determination of embryonic body planning, particularly for the laterality.

Key words: microtubule • kinesin • *kif3A* • gene targeting • left-right asymmetry

INTRACELLULAR trafficking is one of the fundamental mechanisms for maintaining cellular organization by distributing the molecules properly to the lieu where they are required. In the case of neurons, this transportation system is highly differentiated and is termed axonal transport (Grafstein and Forman, 1980; Hirokawa, 1993) in accordance with their highly polarized structure. To carry out these tasks, three major kinds of cytoskeleton-associated motor proteins are recognized today: kinesin superfamily proteins (KIFs)[1] (Aizawa et al., 1992; Hirokawa, 1996, 1998), dynein superfamily proteins (Gibbons et al., 1994; Tanaka et al., 1995; Gibbons, 1996), and unconventional myosins (Fath and Burgess, 1994; Wang et al., 1996). All of these motor proteins exert their force by hydrolysis of ATP, although the track for the former two is microtubules (MTs) while the latter one slides along the microfilaments composed of actin. Among them, KIFs comprise several dozens of molecules that take part in various processes including axonal transport (Kondo et al., 1994; Okada et al., 1995; Yamazaki et al., 1995), intracellular traffic such as intraciliary-flagellar transport (IFT; Kozminski et al., 1995; Morris and Scholey, 1997; Cole et al., 1998), and cell division (Boleti et al., 1996).

Address correspondence to Nobutaka Hirokawa, Department of Cell Biology and Anatomy, University of Tokyo, Graduate School of Medicine, 7-3-1, Hongo, Bunkyo-ku, Tokyo 113-0033 Japan. Tel.: 81-3-3812-2111, ext. 3326. Fax: 81-3-5802-8646. E-mail: hirokawa@m.u-tokyo.ac.jp

1. *Abbreviations used in this paper:* AP, alkaline phosphatase; dpc, days post coitum; ES, embryonic stem; IFT, intraciliary-flagellar transport; KIF, kinesin superfamily protein; MT, microtubule; RT, room temperature; VEC-DIC/FL, simultaneous observation of video-enhanced contrast DIC and fluorescent images.

KIF3A protein is one of the authentic murine KIFs discovered by our PCR screening (Aizawa et al., 1992) that takes on heterotrimers with KIF3B (Kondo et al., 1994; Yamazaki et al., 1995) or KIF3C (Muresan et al., 1998; Yang and Goldstein, 1998) and an associated molecule KAP3 (Yamazaki et al., 1995, 1996), which are in toto called KIF3 complex. Both KIF3A/B have ATPase activity at their NH_2-terminal head region followed by a coiled-coil stalk region assumed to be responsible for dimerization and a COOH-terminal tail domain. Previous biochemical studies (Kondo et al., 1994) have revealed that KIF3A is expressed ubiquitously but predominantly in brain, testis, and adrenal medulla. Furthermore, it has been biochemically revealed that only KIF3A can exist in a soluble form in the absence of its counterpart (Yamazaki et al., 1995) and can form heterodimers with either KIF3B or KIF3C (Yamazaki et al., 1995; Muresan et al., 1998; Yang and Goldstein, 1998), whereas KIF3B aggregates under physiological conditions in the absence of KIF3A in the baculovirus expression system and does not dimerize with KIF3C. Moreover, developmental expression of the KIF3A protein precedes that of KIF3B. Recently, we have made *kif3B* knockout mice (Nonaka et al., 1998) and revealed that KIF3B is essential in early developmental stages, especially for left-right (L-R) determination. From another standpoint, KIF3 has diverse orthologues among species such as sea urchin kinesin II (Cole et al., 1993), *Chlamydomonas* FLA10 (Walther et al., 1994), *C. elegans* Osm3 (Shakir et al., 1993), and a fish photoreceptor KIF3 antigen (Beech et al., 1996). Considering all the aforementioned properties of KIF3A, this molecule proper must therefore have essential and regulatory roles in various animals, and it is anticipated that more severe phenotype shall be observed in the *kif3A* gene-targeting mice.

To pave the way into the investigation of murine KIF3A in situ, we disrupted the murine *kif3A* gene by homologous recombination. The resulting *kif3A*$^{-/-}$ mice displayed severe developmental defects at the mid-gestational stage and died before 10.5 dpc (days post coitum). The defects were mainly localized to the neural tube, heart, brachial arches, and lower truncal mesoderm, leading to highly underdeveloped posterior structures. Surprisingly, the cardiac looping was randomized, i.e., ~40% of all homozygote embryos exhibited a L-loop pattern (situs inversus). Because it has been predicted that the node plays an important role in L-R determination, we examined the node of *kif3A*$^{-/-}$ and compared it with that of wild-type embryos. Since *Chlamydomonas* orthologue FLA10 has been reported to be localized in the motile flagella as a motor for the IFT (Kozminski et al., 1995; Cole et al., 1998; Rosenbaum et al., 1999), we also focused our attention on the monocilia of the embryonic node. In the wild-type embryos, the monocilia of nodal pit cells are motile and generate a leftward flow of extraembryonic fluid (nodal flow). However, formation of cilia on the surface of nodal pit cells was severely affected and no flow was recorded in *kif3A*$^{-/-}$ homozygous embryos. These data suggest the possibility that KIF3A molecules are involved in the initial determination of the L-R asymmetry by contributing to formation of cilia, which generates leftward flow of the extraembryonic fluid. In addition, the lack of nodal cilia might bring about abnormal distribution of mesoderm-inducing activity such as *sonic hedgehog* (*shh*), and homozygous embryos displayed disturbed mesodermal structures.

Materials and Methods

Generation of the Targeting Vector

A 20-kb genomic fragment containing full-length *kif3A* was selected from a murine genomic library of embryonic stem (ES) cell line J1 (Tanaka et al., 1998) and probed using a mouse cDNA fragment encoding the P-loop exon of *kif3A* (Kondo et al., 1994). The two independent phage clones obtained were cloned into pBS (Stratagene) vector. These clones were subsequently subcloned into pBS and mapped by a combination of several restriction enzymes and partial sequencing. We applied the conventional positive-negative selection (Yagi et al., 1993) together with the poly(A) trap strategy. As shown in Fig. 1 A, we applied a 1-kb-long HindIII-SalI fragment as a 5′-homologous arm and a 5-kb-long fragment as a 3′-homologous arm. Then poly(A)-less pGKneo positive selection cassette was flanked by these arms and cloned into a modified multiple cloning site in the DT-A cassette B vector (GIBCO BRL). Finally, this construct was prepared on a large scale with a QIAGEN miniprep kit. This plasmid was linearized by NotI and an appropriate concentration of vector (25 μg/ml) was prepared for the subsequent transfection into ES cells.

Transfection and Screening of Recombinant ES Clones

We have performed the electroporation of targeting vector to J1 cell line basically according to Harada et al. (1994) with a slight modification in G418 concentration. After electroporation, the transfected cells were selected in the presence of G418 (GIBCO BRL) at a concentration of 175 μg/ml. About 10 d after electroporation, the growing positive selected colonies of ES cells were picked up in duplicated 96-well plates, one for cell stock and the other for genomic DNA preparation. Screening of recombinants was performed by genomic Southern blotting with ^{32}P-radiolabeled external probe (generated by PCR ~0.4 kb) as indicated in Fig. 1. Then the integrity of candidate clones was further confirmed with an internal and *neo* probes (data not shown). Three independent recombinants out of ~450 ES colonies were obtained by this poly(A) trap targeting strategy. These recombinant clones were injected into the blastocysts recovered from superovulated C57BL/6N line and raised chimeric mice from two independent cell lines. We identified chimeric mice by contribution of agouti coat color. Male chimeras were bred with C57BL/6J to obtain heterozygous offspring, from the mating of which we could obtain *kif3A* null mutants.

PCR Genotyping

The generated mice were routinely probed by PCR for the identification of their genotype as described previously (Tanaka et al., 1998). In brief, a small portion of mouse tail was incubated in a tail lysis buffer (10 mM Tris-HCl, 25 mM EDTA, 1% SDS, and 75 mM NaCl, pH 8.0) supplemented with 100 μg/ml proteinase K (Merck). The Eppendorf tubes containing these samples were shaken in an air incubator maintained at 55°C overnight. Phenol-ethanol extraction and ethanol precipitation were performed before the PCR reaction. About a hundredth amount of each purified DNA was routinely used for PCR. The following two pairs of primer sets were used for genotyping offsprings: (a) neo primers, neoF (1620–1649) 5′-TGG GCA CAA CAG ACA ATC GG-3′, neoR, (1841–1820) 5′-ACT TCG CCC AAT AGC AGC CAG-3′; (2) internal primers, kif3A-F4, (346–369) 5′-TGT TCC ATA TAG CCC AGG ATA CCC-3′, kif3A-B1, (545–525) 5′-GAT GGT CCC TGA AAA TGG TGC-3′.

To determine the embryonal genotype, we collected amniotic membranes. They were dissolved in aqua destillata supplemented with 100 μg/ml proteinase K under shaking at 55°C for 1 h. A small amount (2 μl) of the lysate was used for PCR amplification.

Western Blotting of the Embryos

The whole embryos ranging from 9.5 to 10 dpc were killed and minced by using a pair of ophthalmological scissors in PBS supplemented with protease inhibitor cocktails (5 mM PMSF, 10 ng/ml leupeptin, pepstatin, benzamidine, and 100 mM DTT; Wako Pure Chemicals Co.) on ice. By using a Potter's homogenizer, small pieces of embryos were completely de-

stroyed. The resultant homogenate was centrifuged at 15,000 rpm by using a Beckman TL-100 for 30 min and the supernatant was collected. The protein concentration of each sample was adjusted to 10 μg/ml and used for standard Western blotting procedure as described previously (Tanaka et al., 1998). Here we used the following antibodies to ascertain the expression level of KIF3A and KIF3B proteins in the mutant mice: both monoclonal and polyclonal anti-KIF3A antibodies (Kondo et al., 1994), and polyclonal anti-KIF3B antibody (Yamazaki et al., 1995).

Preparation of Embryos for Light Microscopy

The embryos dissected from the pregnant mice were processed for the light microscopic observation by the following method. As soon as the embryos were extirpated from the uterus, a small portion of extraembryonic membranes was retained for the determination of genotype by PCR and the embryos proper were soaked into Bouin's fixative (75% pycric acid, 5% glacial acetic acid, and 25% formaldehyde; Wako Pure Chemicals Co.). After fixing embryos for 2 h at room temperature (RT), the samples were dehydrated by a graded series of ethanol solutions, followed by substitution of xylene. Finally, the whole mount embryos were placed in melted Paraplast (Oxford Labware) at 65°C for ~90 min with two changes of this embedding material. The samples were embedded in fresh Paraplast after complete penetration of the samples by the embedding material. The blocks were cut by using a rotatory microtome (HM355; Carl Zeiss) into 7-μm-thick serial sections, then the sections were mounted onto glass slides, which were in turn deparaffinized and stained with hematoxylin and eosin according to Kaufman (1995) with slight modifications. These sections were observed and photographed by a Nikon Optiphot-2 microscope.

Preparation of Embryos for Scanning Electron Microscopy

The dissected embryos were fixed by using half Karnovsky solution (2% paraformaldehyde and 2.5% glutaraldehyde in 0.1 M cacodylate buffer, pH 7.2) for 2 h at RT. Then we soaked these embryos into 10% sucrose solution buffered by 0.1 M cacodylate for 20 min, followed by postfixation with 1% osmium tetraoxide in cacodylate buffer on ice for 15 min. After washing the embryos extensively with aqua destillata, dehydration with a graded series of ethanol solutions was performed. After completing the dehydration process, the media was substituted with isoamyl acetate and the embryos were left to stand in this solution at RT for over 30 min. They were then prepared for scanning electron microscopy by critical point freeze-dry procedure as described previously (Nonaka et al., 1998). In brief, they were soaked into liquid carbon dioxide under high pressure (JCPD-5; JEOL). Then the chamber was gradually heated to the critical point, where the embryos could be dried without being destroyed. The samples obtained were surface-coated using a gold spattering device (JSM-5200; JEOL) under the optimal conditions for 10 min. The samples were viewed under a JEOL scanning electron microscope (JEM2000) at 100 kV and photographed by a Polaroid.

Transmission Electron Microscopy of the Nodal Monocilia

Embryos at 7.5 dpc were dissected out from the uterus and were fixed by the method of Mizuhira and Futaesaku (1972) to obtain good preservation of axonemal proteins. Then the samples were processed and observed routinely as described previously (Takeda et al., 1995).

Whole Mount In Situ Hybridization

Whole mount in situ hybridization of the mouse embryos other than *lefty-2* was carried out principally according to Conlon and Rossant (1992) with several modifications. In brief, the embryos were dissected in sterilized RNase-free PBS and fixed with 4% paraformaldehyde not equilibrated with NaOH at 4°C. After incubation for 2 h, they were washed twice with PBT (PBS supplemented with 0.1% Tween 20), followed by bleaching with PBT and 30% hydrogen peroxide. They were then treated with proteinase K (10 μg/ml; Merck) for several minutes at RT. Embryos were further fixed with 0.2% glutaraldehyde containing 4% paraformaldehyde, prehybridized, and then hybridized with appropriate markers (overnight, 70°C). On the following day, the sample embryos were washed with buffers and treated with RNase to remove unbound or nonspecific binding probes. After that, alkaline phosphatase (AP)–conjugated anti-DIG antibody (Roche Diagnostics) was applied and incubated overnight at 4°C. On the next day, the embryos were washed with TBST (Tris-buffered saline containing 0.2% Tween 20) with medium changes every 1 h. The washing process continued into the following day when the final AP color reaction was performed. The reaction was carried out according to the standard method (NBT and BCIP; Roche Diagnostics) and the color reaction was stopped whenever the localization of markers became clear and distinct. We have performed a series of dehydration/rehydration processes (Hogan et al., 1994) to darken the color of the AP reaction precipitate products. The embryos were then soaked in a glycerol/TBST solution to make the body transparent for easier identification of staining at a three dimensional level.

For staining the embryos by using the *lefty-2* probe, we followed our previous method (Nonaka et al., 1998).

Nodal Cilia Motility Assay

Nodal cilia can be observed during the nodal formation and bulging at 7.5 dpc (Nonaka et al., 1998). The lower halves of the embryos dissected from the uterus were eliminated by using a pair of electrolytically sharpened tungsten needles. The half-egg like structure was embedded into a small hole of silicon-rubber membrane (thickness ~300 μm) attached onto the surface of a glass slide. Another silicon membrane having a hole at its center (diameter ~5 mm) was overlaid onto it. We filled the hole with motility solution (50% heat-inactivated rat serum, 49% DMEM and 1% 1 mM sodium pyruvate) and sealed it by simply placing a coverslip on it. Fluorescent beads (Fluosheres, carboxylate-modified microspheres; Molecular Probes) with a diameter of ~220 nm were added to the assay solution to ~5% for visualization of flow generated by the motile cilia. The preparations were viewed under VEC-DIC/FL microscopy (Olympus Inc.) and a series of motility assay was videotaped simultaneously. The embryos under investigation were genotyped after observation.

Immunocytochemistry of the Nodal Cilia and the Embryo Section

Embryos were fixed with 4% paraformaldehyde and processed by a standard cryosectioning method. The blocks were sectioned with a Leica cryomicrotome, and extended on the surface of glass slides. The samples were permeabilized with 0.1% Triton X-100 and blocked with 5% skim milk followed by a standard immunocytochemical procedure as described elsewhere (Nonaka et al., 1998). For the staining by anti-axonemal dynein antibody, we generally followed the method of Umeda et al. (1995) with slight modifications. The stained preparations were examined under a confocal laser scanning microscope (Bio-Rad).

Results

Targeting Strategy and Confirmation of Homologous Recombination

Initially, we tried to obtain homologous recombinants by using a standard positive-negative selection vector and screened ~800 ES cell colonies. However, we could not successfully obtain any recombinant clones, which led us to adopt the poly (A) less pGK-neo cassette with an A-T rich/pausing signal (Fig. 1 A). Under this condition, three independent clones out of ~450 colonies were isolated, all of which have been used for blastocyst injection. As shown in Fig. 1 B, wild-type embryos displayed a single 3.2-kb fragment when digested with EcoRI, while an additional 2.1-kb band was observed in heterozygotes by genomic Southern blotting. Another restriction enzyme (XbaI) being diagnostic for targeting events, also verified successful homologous recombination (data not shown). Genotypes were also identified by PCR where primer pairs explicitly detect the targeted events. As represented in Fig. 1 D, almost all littermates of heterozygous mothers intercrossed with male heterozygotes revealed proper separation of genotype according to Mendel's law. We made a necropsy

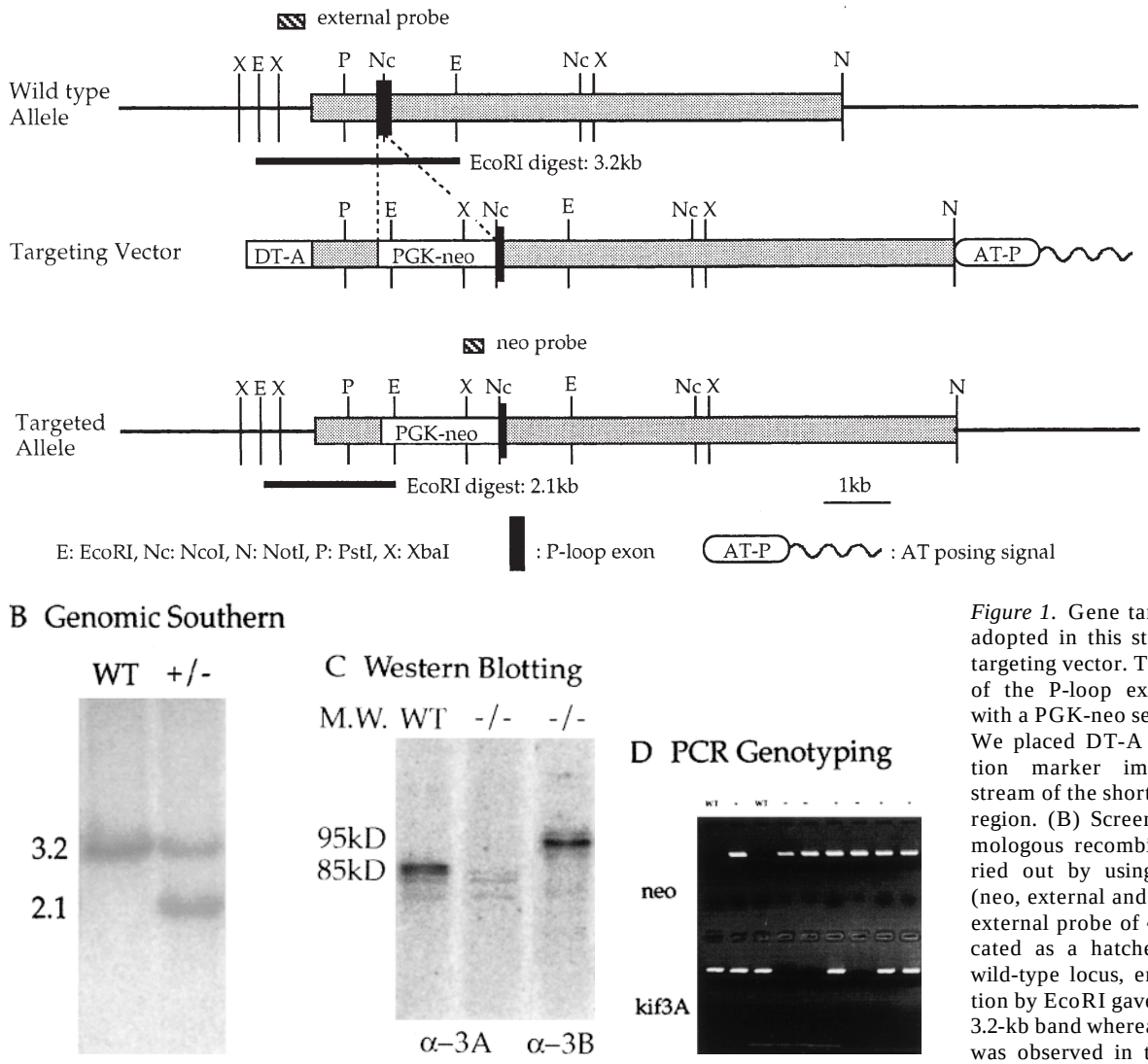

Figure 1. Gene targeting strategy adopted in this study. (A) Gene targeting vector. The anterior half of the P-loop exon is replaced with a PGK-neo selection marker. We placed DT-A negative selection marker immediately upstream of the short arm consensus region. (B) Screening of the homologous recombinants was carried out by using three probes (neo, external and internal). Only external probe of ~0.4 kb is indicated as a hatched box. In the wild-type locus, enzymatic digestion by EcoRI gave rise to a single 3.2-kb band whereas a 2.1-kb band was observed in the case of the knocked-out allele. (C) Western blotting of the whole embryos killed at 9.5 dpc revealed no KIF3A band in homozygotes while KIF3B was still expressed. (D) PCR analysis of littermates. Null mutant homozygous embryos do not generate any bands by primer set #2 while #1 (neo) produced a single distinct band.

of 20 pregnant heterozygotes expected to have homozygote offsprings during 7.5–11.5 dpc, which revealed that no homozygotes were observed after 10.5 dpc (Fig. 1 D, Table I), suggesting the midgestational lethality of homozygous embryos. Western blotting analysis of all littermates revealed a complete absence of KIF3A protein from homozygous mice. Interestingly, KIF3B protein, being a counterpart in the KIF3 complex, was expressed at a normal level (Fig. 1 C, lane 3).

Severe Developmental Abnormalities in kif3A$^{-/-}$ Mice

kif3A homozygotes were generally smaller compared with heterozygous and wild-type littermates at 9.5 dpc. Furthermore, no living embryos were obtained when cesarean section of pregnant mice was carried out after 11 dpc (Table I). At 9.5 dpc, the homozygotes displayed severe malformation characterized by swelling and degeneration of the neural tube (Fig. 2 and see Fig. 5, B and D) mimicking the phenotype of hydrocephalus. Furthermore, extreme distension of the pericardium due to pericardial effusion was noted. A regular array of somites as seen in wild-type embryos (see Fig. 5 A) could not be observed in homozygote embryos (see Fig. 5 C), simply showing degenerated bulk in the lower truncal part and abnormal somitegenesis, i.e., sirenomelia. In most cases, embryonic turning was not completed at 9.5 dpc, suggesting growth retardation/inhibition of the homozygotes. Staggering of the neural tube

Table I. Genotype Separation of Offspring after Mutual KIF3$^{+/-}$ Mating

Age	Wild-type	+/−	−/−	ND	Total
E7.5	12	23	12	4	51
E8.0–8.5	20	41	18	8	87
E9.5	9	21	12	0	42
E10.5	14	29	6	0	49
E11.5	9	17	0	0	26
Adult	52	90	0	0	142

Allelic separation of embryos at various stages. Until 9.5 dpc, clear Mendelian separation was encountered while homozygous mice started to die at ~10.5 dpc. No homozygotes could be encountered after 11 dpc.

was prominent at this incomplete turning region. These phenotypes are suggestive of disturbed mesodermal development resulting in failure of neural tube induction. In addition, the severity of the phenotype observed at 9.5 dpc was almost correlated with the expression level of the KIF3A molecule, which revealed relatively strong signal intensity in the neural tube (see Fig. 4 B, Nt) and the heart (idem, Cor).

Moreover, we encountered abnormal heart looping. In wild-type cases (Fig. 3, A and D), almost 100% of embryos displayed a D-loop pattern while a few atypical phenotype also existed. On the contrary, in homozygotes, ~40% of the embryos revealed a L-loop type heart (Fig. 3, C and F). In some cases (~20%), incomplete cardiac looping, i.e., a tuba rectae, was observed. These results suggested that randomization of the heart looping occurred in *kif3A* homozygous mice. To address this point more precisely, we scrutinized these embryos with *lefty-2* RNA probe, to see whether it involves abnormal *lefty-2* expression, as *lefty-2* product is considered to be one of the earliest left-right determinant in early murine development (Meno et al., 1997, 1998). As has been observed in our previous report for *kif3B*$^{-/-}$ (Nonaka et al., 1998), the expression of *lefty-2* was bilateral or downregulated in *kif3A*$^{-/-}$ embryos (see Fig. 6 B). In some cases, the expression was extended to the contralateral paraxial mesoderm (Fig. 6, the right two) while normal pattern still existed (Fig. 6 B, the left-most embryo). On the contrary, almost all wild-type embryos and heterozygotes displayed normal left-side restricted pattern (Fig. 6 A). Regarding a cardiogenesis, hypoplasia of the myocardium was another striking feature of *kif3A* homozygous embryos. A sagittal section of the heart wall indicated fairly underdeveloped myocardium (Fig. 6 E) compared with normal embryos (Fig. 6 F), which might be a cause of circulatory insufficiency in utero.

No Cilia Were Formed in the Node of 7.5 dpc kif3A$^{-/-}$ *Embryos*

The node is normally formed at 7.5 dpc and is essential for further induction of mesodermal anlage and in turn for neural tube formation. As *Chlamydomonas* orthologues of the KIF3 complex have been reported to engage in IFT (Kozminski et al., 1995; Cole et al., 1998; Rosenbaum et al., 1999), we focused on the ciliated mesodermal cells which normally accommodate monocilia (Sulik et al., 1994). As shown in Fig. 7, A and B, the nodal region forms a small dimple at the base of the dorsal part of embryo where the cell density is quite high. Since the cells constituting the node are smaller than surrounding endodermal cells at this developmental stage, this region could readily

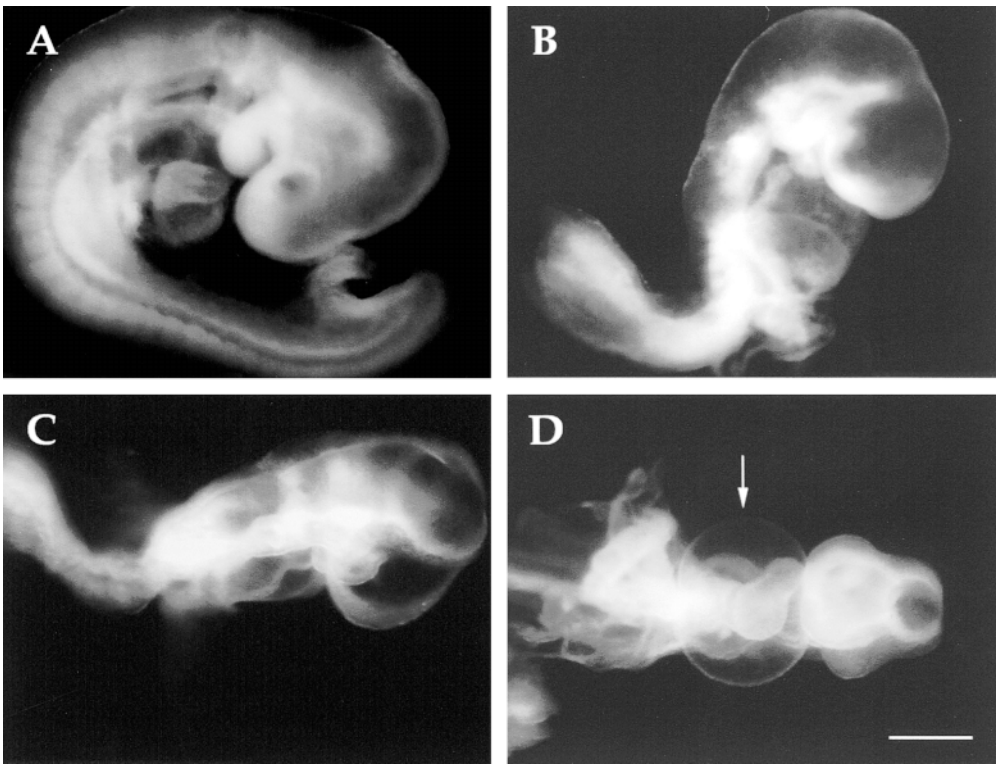

Figure 2. Macroscopic overview of both wild-type and homozygous embryos at 9.5 dpc. (A) Lateral view of a wild-type embryo. Normal development of somites and the nervous system can be observed. (B) Same view of a homozygous embryo. Note the severe degeneration of the lower half of the body accompanied by thin neural tube wall. (C) Dorsal view of a homozygous embryo, exhibiting a staggered midline structure with disorganized somites. (D) Extensive pericardial effusion (arrow) resulting in circulatory insufficiency. Bar, 1 mm.

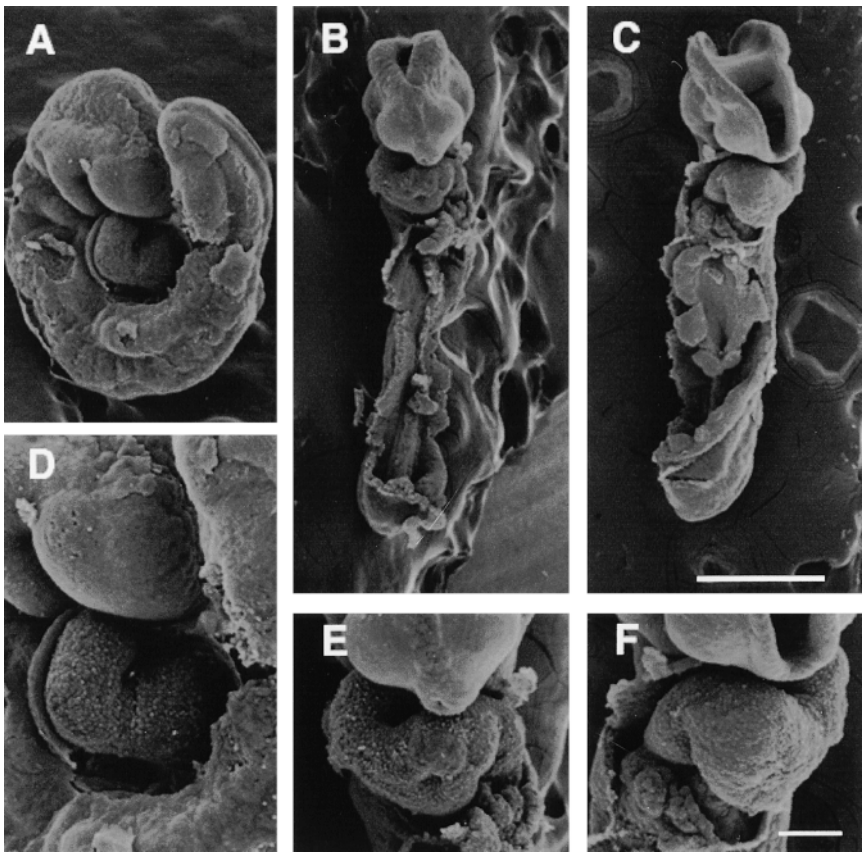

Figure 3. Scanning electron microscopy of the embryos at 8.5 dpc. Wild-type embryo displays normal body turning (A) and heart loop (D, D-type) while homozygotes (B and C) did not make turning. Some homozygotes exhibited inversed heart looping (F, L-type). In addition, seemingly normal heart of homozygote (E) display irregular cardiac surface as seen in F. Bars: (A–C) 500 μm; (D–F) 100 μm.

be discriminated from other parts of the embryonic body. At a glance, the wild-type/heterozygous cells normally exhibited cilia ranging from 2 to 4 μm in length and having pinpoint-like ends (Fig. 7 C). However, in the case of *kif3A*$^{-/-}$ mice (Fig. 7 D), the surface structure displayed quite striking differences. There were almost no mature cilia, although there existed some very short rudimentary processes. This phenotype was invariably observed among

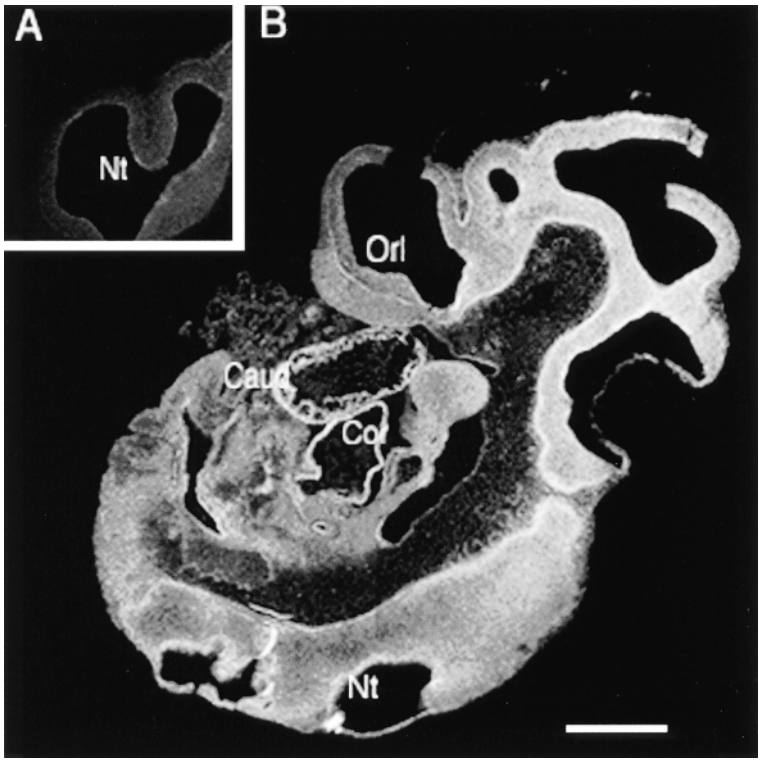

Figure 4. Expression pattern of KIF3A molecule in 9.5 dpc embryos (B). Expression of the KIF3A molecule is almost ubiquitous although we can recognize relatively strong accent in the neural tube (Nt) and the heart (Cor). Orl, oral cavity; Caud, caudal region. (A) Control panel stained with preimmune serum. Bar, 1 mm.

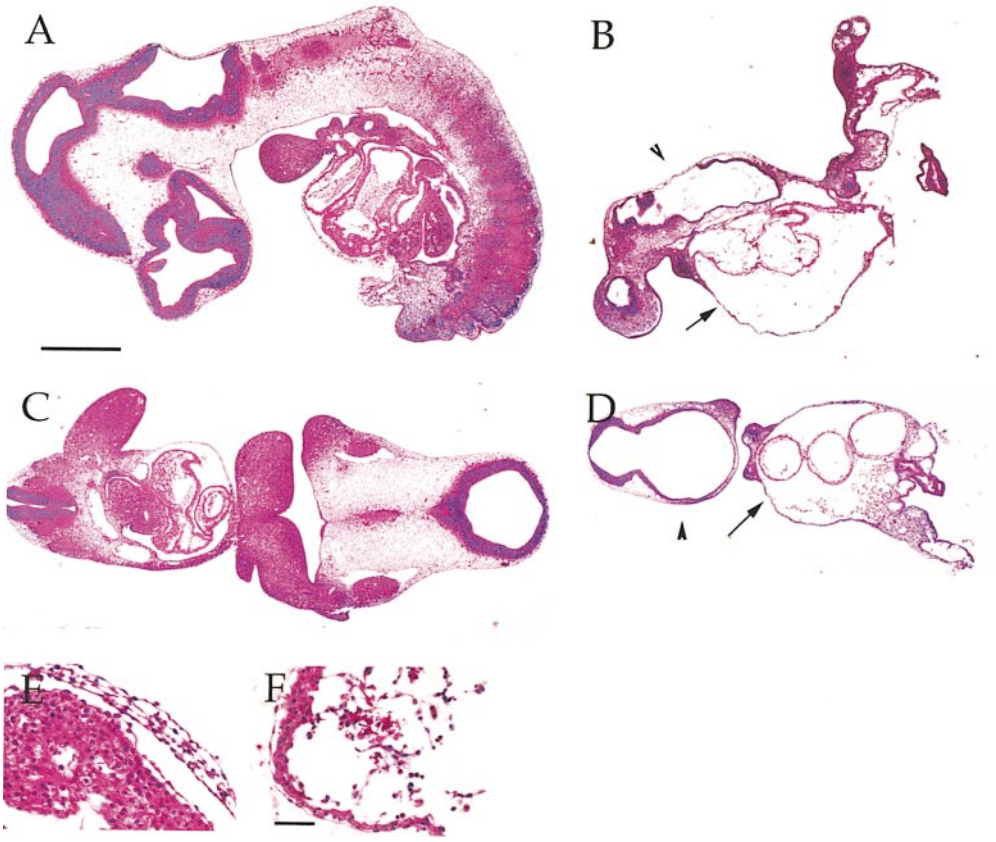

Figure 5. Histological analyses at 9.5 dpc stained by the HE method. Sagittal section of a wild-type (A) and a homozygous (B) embryo. Systemic hypoplasia, extended pericardium (arrows) and thinning of neural tube wall (arrowheads) are characteristic to the homozygotes. Frontal sections of both type of embryos (C, wild-type; D, homozygote) display striking differences as described in the sagittal sections. Cardiac insufficiency in homozygotes is partly explained by the hypoplastic myocardium (F). Note the well-developed myocardial wall in the case of wild-type (E) embryos. Bars, 1 mm.

homozygous mouse littermates, suggesting the possible role of the KIF3A molecule in constructing and maintaining the monocilia structure.

The KIF3A-null Mutant Embryos Were Defective of the Leftward Extraembryonic Nodal Flow as Revealed by Fluorescent Beads

To decipher the degree of dysfunction of nodal pit cell cilia in *kif3A*$^{-/-}$ embryos, we have carried out a motility assay. An embryonic body harboring a node was placed under the VEC-DIC/FL microscope and fluorescent beads were added to the solution surrounding the embryos. By using this method, we can simultaneously observe both ciliary movement and nodal flow. In wild-type and heterozygous embryos, distinct flow generated by the rotating cilia was recorded and this flow was directed leftward with reference to the presumed body A-P axis (Fig. 8 A). This regular flow was especially evident in the posterior part of the node. On the contrary, in KIF3A-deficient embryos, we could identify no such a regular flow, while rather Brownian movement of beads was observed (Fig. 8 B). This result clearly indicates that the cilia of nodal pit cells is involved in gradient formation within the nodal groove, implying some important roles of the KIF3A molecule in the determination of early body planning.

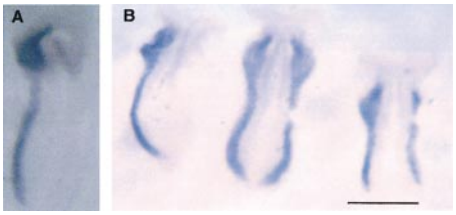

Figure 6. Whole mount in situ hybridization of embryos probed with lefty-2. As represented in A, almost all wild-type and heterozygous embryos expressed *lefty-2* mRNA at the left paraxial mesoderm. In homozygotes (B), certain extent of embryos exhibited *lefty-2* on both sides while there still exist embryos expressing it only on the leftside. Bar, 1 mm.

We have carried out immunostaining of nodal cilia to determine whether KIF3A molecules are really installed in the motile cilia. Cryosection of the node stained with anti–α-tubulin (DM1A) indicates the presence of cilia containing MT cytoskeleton (Fig. 8, B and D). Double immunostaining of the same embryo with an anti-KIF3A antibody revealed the localization of KIF3A molecule within the cilia (Fig. 9 A), suggesting that the KIF3A molecule might be engaged in the construction and maintenance of the ciliary structure. These results are almost the same as those obtained from the KIF3B-deficient embryos (Nonaka et al., 1998), strongly suggesting that KIF3A is really a counterpart of KIF3B in vivo. Collectively, KIF3A molecules may be essential for ciliary formation, determining the subsequent developmental cascades.

Moreover, staining with an anti-outer axonemal dynein antibody (AD2; Yoshida et al., 1989) and anti-axonemal dynein intermediate chain (IC140; Yang and Sale, 1998) also revealed the presence of this molecule within the monocilia (Fig. 9, C and E). Because the nodal area is composed of several optical sections by confocal laser

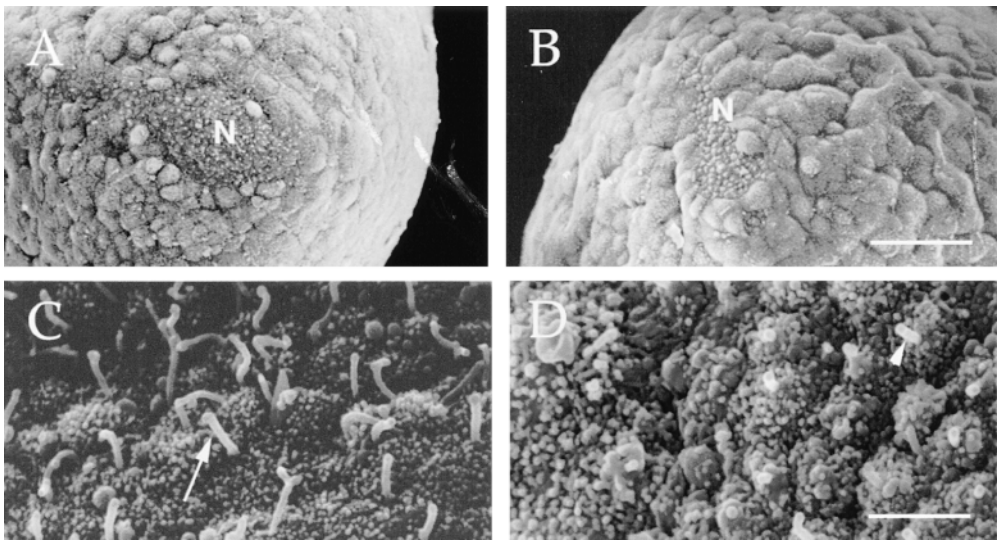

Figure 7. Scanning electron microscopy of the node (N) of a wild-type embryo (A) and a homozygote (B). Single cilium (arrow) on each nodal cells can be observed in the wild-type embryo (C) while no or extremely short cilia were present in the homozygote (D). Bars: (A and B) 50 μm; (C and D) 5 μm.

scanning microscopy while that for cilia is made of a few sections, the background fluorescence in the nodal area seems to be higher. However, as there are no positive staining of cilia in the negative control panel (Fig. 9 G), we could state that the localization of ciliary axonemal dynein is specific. We could also identify both inner and outer arm dynein localizing on the surface of doublet MTs with in the monocilia (arrows for inner arm dynein and for outer arm dynein, Fig. 9, I and J) by a conventional electron microscopy. These results collectively imply that axonemal dynein is a candidate cargo of KIF3A that may in turn be engaged in the movement of monocilia.

Shh Expression Was Somewhat Reduced in Mutant Rostral Portion

As both development of the mesodermal structure and the determination of L-R asymmetry were highly affected in the *kif3A*$^{-/-}$ mice, we also examined the expression pattern of some developmental markers for delineating the role of the KIF3A molecule in this process. *Pax6* (Jordan et al., 1992) expression in 9.5 dpc embryos did not exhibit any apparent changes in the eyes except for slightly reduced expression in the forebrain (Fig. 10, A and B). *Brachyury* (*T*, see review by Willison, 1990) is a mesodermal marker that is normally expressed in the midline structures with a strong accent at the tail bud region. At 8.5 dpc, its expression patterns in both embryos (wild-type; Fig. 10 C, homozygote; Fig. 10 D) were very similar, but midline staining corresponding to the notochord was fainter in the case of homozygous embryos. Of noteworthiness, another midline mesodermal marker, *sonic hedgehog* (*shh*; Conlon et al., 1995), exhibited the most dramatic change in homozygote embryos even at early developmental stage (7.5 dpc, Fig. 10 G). Normally, this marker is expressed in the node, notochord and subsequently in the floor plate. Furthermore, the ventral half of the mesencephalon also expresses it resulting from induction by the underlying floor plate at this region (Ekker et al., 1995). In the case of homozygous embryos (Fig. 10, E and F, lower embryos), the expression of *shh* at the thoracic notochord was significantly reduced and the staining per se became staggered to a certain extent. Moreover, the expression in the mesencephalon was completely absent in homozygous

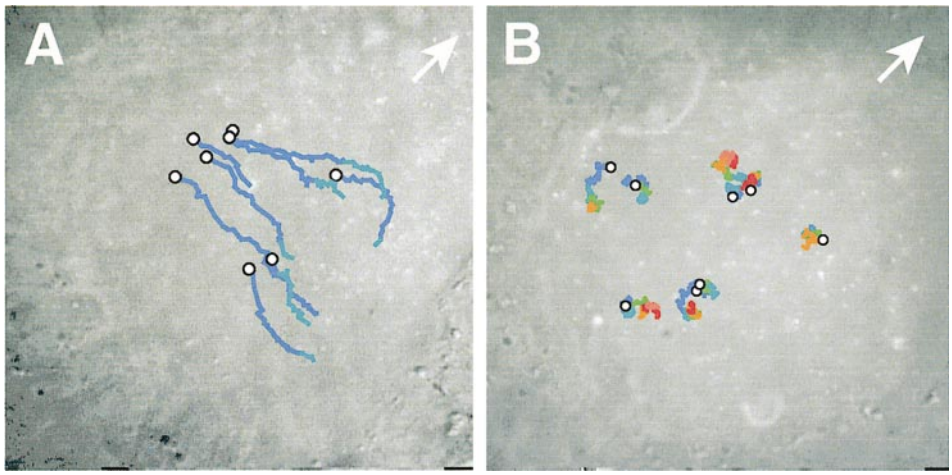

Figure 8. Ciliary movement assay. (A) Leftward nodal flow was observed in the case of wild-type embryos ($n = 3$). (B) In *kif3A* null mutants ($n = 5$), only Brownian movement of fluorescent beads was observed, which was markedly different from regular flow. Bars, 5 μm.

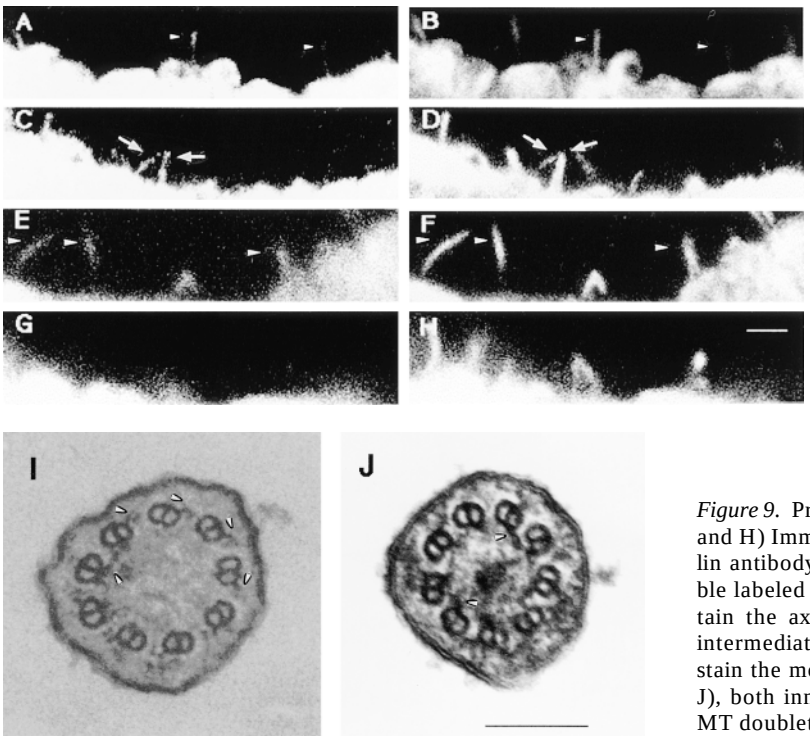

Figure 9. Presence of axonemal dynein within monocilia. (B, D, F, and H) Immunostaining of nodal cilia at 7.5 dpc with anti–α-tubulin antibody. Nodal cilia (arrowheads) were identified and double labeled with anti-KIF3A antibody (A). These cilia also contain the axonemal outer arm dynein (C, arrows) (AD2) and intermediate chain (IC140, E) while negative control (G) did not stain the monocilia. By transmission electron microscopy (I and J), both inner and outer arm dynein localize on the surface of MT doublets (arrowheads). Bars: (A–H) 5 μm; (I and J) 100 nm.

mice (Fig. 10 E, lower embryo) while abundant expression could be encountered in wild-type embryos (Fig. 10 E, upper embryo). This absence of *shh* expression in brain structures might result in abnormal development of the neural tube, leading to the hydrocephalus-like phenotype and neural tube hypoplasia. Actually, exencephaly (Fig. 3 C) was relatively frequently observed in our *kif3A* null mutants under the genetic background with lesser contribution of C57BL/6J, suggesting the possibility that some modifier loci of this phenotype are present in the 129/Sv strain. In addition, reduced expression of *shh* in the rostral region together with reduced *T* expression in the truncal part collectively suggest the influence of the KIF3A molecule in the formation of A-P axis possibly through transporting inductive signals or their receptors.

Discussion

In summary, this is one of the first reports describing the general function of the KIF3 complex in vivo. The null mutant embryos displayed smaller body size and early developmental failure characterized by mesodermal hypoplasia and degeneration followed by the development of neural tube defects. Furthermore, determination of L-R asymmetry was randomized, exhibiting the phenotype represented by L-loop formation of the cardiac tube (situs inversus). This phenotype was presumably due to defective nodal cilia as identified in our previous *kif3B* mutant (Nonaka et al., 1998). These results reinforce our biochemical data that KIF3A is a counterpart of KIF3B (Yamazaki et al., 1995). Another new idea on the function of KIF3A is that it is involved in mesodermal formation, which then regulates the development of neural tissues. Here we should like to discuss the possible role of the KIF3A molecule with special reference to (a) the early developmental events and (b) the determination of laterality.

KIF3A and Early Developmental Sequella

KIF3A is reported to be already expressed in ES cells and precedes that of KIF3B. Considering the biochemical data that KIF3A could remain soluble in the absence of its counterpart (Yamazaki et al., 1995), the earlier death of *kif3A*$^{-/-}$ embryos than that of *kif3B* homozygous embryos (no surviving embryos after 11.5 dpc; Nonaka et al., 1998) is quite reasonable. Although the macroscopic phenotype was not so evident until 8.5 dpc in *kif3A* null mutants, microscopical changes in *kif3A* homozygotes were even evident early in the node formation stage (7.5 dpc). The node is generally believed to be responsible for the induction of further midline mesodermal structure. The absence of cilia on the surface of nodal pit cells in *kif3A* null mutants and the normal distribution of KIF3A molecules within these cilia in wild-type embryos strongly suggest that the nodal cilia are to some extent constructed and maintained with the aid of KIF3A molecules. Although a previous report suggested the presence of axonemal outer arm dynein in primary cilia (9 + 0 structure, two basal bodies; Umeda et al., 1995) of mammalian sperm and lung ciliated epithelium, and it might be responsible for actual motility, our data presented here and in a previous study (Nonaka et al., 1998) indicated KIF3A and KIF3B are essential for transporting these ciliary components. Axonemal outer arm dynein per se is probably transported down within the cilia as a transporting complex for the following two reasons. On the first line, our immunocytochemical staining clearly demonstrated the colocalization of KIF3A and outer axonemal dynein within monocilia (Fig. 9, C and E). Second-

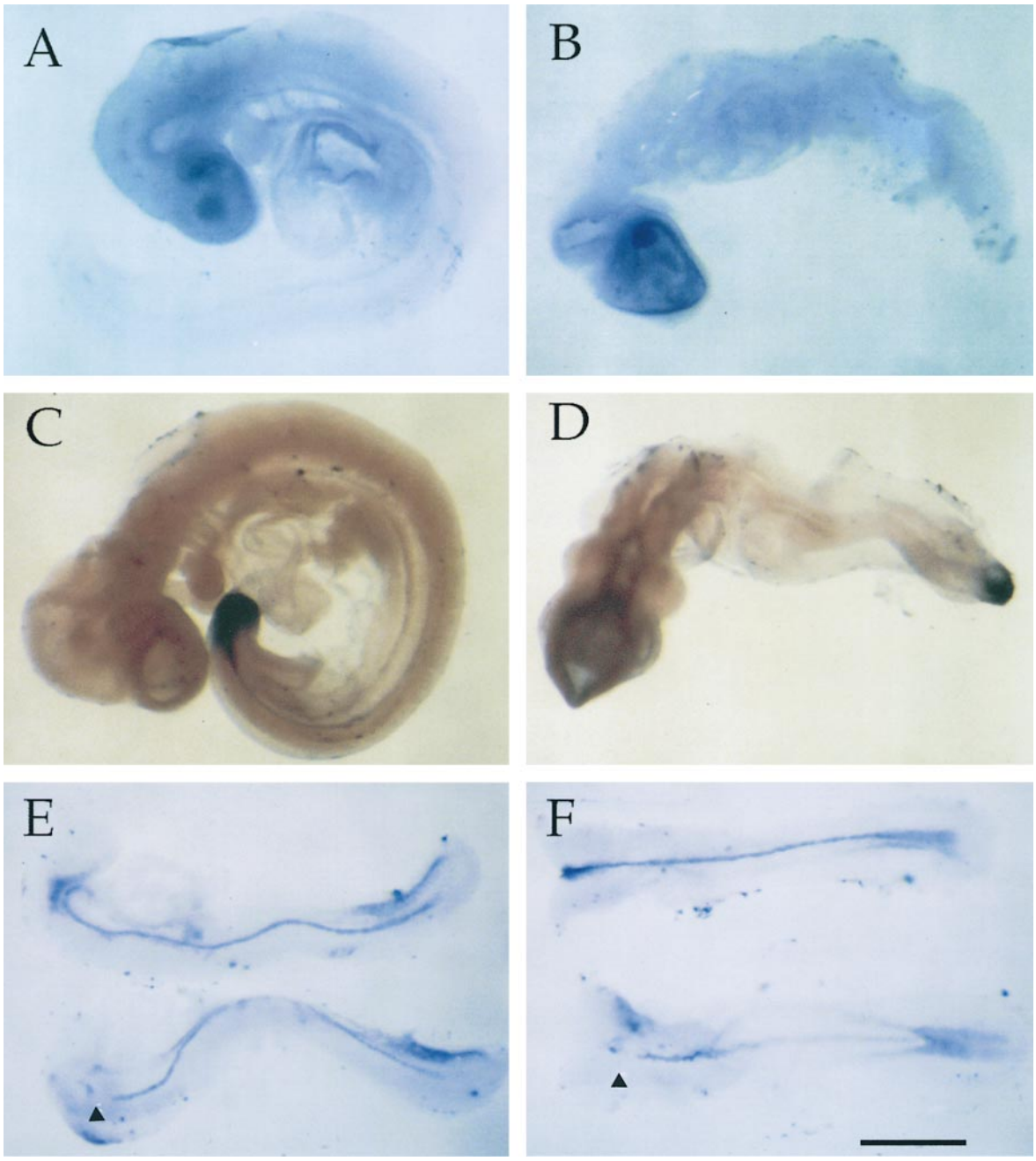

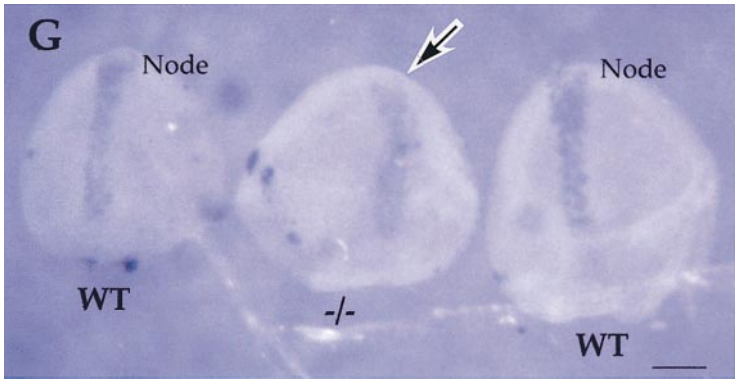

Figure 10. Whole mount in situ hybridization. The wild-type embryos (A and C) and homozygous embryos (B and D) were probed with *Pax6* (A and B) and *Brachyury* (C and D) at 9.5 dpc. In the case of *sonic hedgehog*, lateral view (E) and dorsal view (F) of both wild-type embryos (upper embryos) and homozygous embryos (lower embryos) are presented at 8.5 dpc. Although normal expression pattern of *Pax6* was almost preserved in *kif3A*-deficient embryos while its expression level was downregulated (see text). Expression patterns of *shh* and *T* were significantly altered. Note the absence of *shh* at the mesencephalic region (arrowhead). Some nonspecific deposition of signals can be observed in the head region of the panel (D), which might result from precipitate flow through the distended canalis centralis in mutants. At 7.5 dpc (G), shh expression is dramatically reduced without strong localization within node (arrow) compared with wild-type embryo (Node). Bars: (A–F) 1 mm; (G) 150 μm.

arily, mutations in a putative axonemal dynein heavy chain (*lrd*), being abundantly expressed in these ciliated nodal cells (Supp et al., 1997), de facto resulted in situs inversus. These results are in good agreement with the case of *Chlamydomonas* FLA10, where large IFT complexes are transported by this KIF3 orthologue and depletion of this motor protein resulted in the absence of normal motile flagella (Cole et al., 1998; Rosenbaum et al., 1999).

Then by what mechanism are the early developmental events disorganized, giving rise to multisystem failure? Although there is no direct evidence interfacing the function of KIF3A and early inductive events, it is supposable that the defective nodal cilia could not properly distribute some presumably soluble substances to their proper destinations. Alternatively, intracellular transport of some kinds of receptors to proper direction might be affected. Especially, the abnormal expression pattern of *Brachyury* (*T*) and *sonic hedgehog* (*shh*) could partly explain the hypoplasia of midline structure and degeneration of posterior body structure. The generally accepted idea holds that *shh* is secreted as a complex form bound to cholesterol (Cooper et al., 1998). Considering the size of this complex and cilia, it is reasonable that the lack of cilia resulted in disturbance of orthotopic *shh* expression in *kif3A*$^{-/-}$ homozygote mice. In addition, spontaneous mutation of *shh*, *cyclopia* (Chiang et al., 1996), and targeted disruption of *shh* (Lanske et al., 1996) partly share the phenotypes observed in this *kif3A* null mutant. These ideas collectively imply the relationship between the KIF3 molecule and transport of the Shh molecule.

From another standpoint, as neural induction depends on the mesoderm, abnormal neural tube formation could be attributed to this general failure of anterior development. Indeed, the lack of *shh* staining at the ventral half of the mesencephalon implies that the neural phenotype is partly secondary to mesodermal abnormality. In fact, expression of *shh* at 7.5 dpc in homozygotes is already more altered than that of wild-type embryo, displaying very faint trace amount with no nodal accentuation. However, considering that neuronal morphogenesis also involves cellular movement and assortment by themselves, the neural phenotype might be explained independently by genuine neuronal failure brought about by *kif3A* disruption. In addition, as some reports suggested the presence of cilia on the neuron (Vigh-Teichmann et al., 1980), the neural phenotype may partially be attributable to the lack of neuronal cilia.

Ciliary Movement in Node: Implications for Left-Right Asymmetry

As has been discussed in the previous section, KIF3A might transport materials required for the cilia assembly and maintenance, so that the absence of KIF3A molecules results in ciliary disorganization, leading to several developmental defects. One of the most remarkable phenotypes in these mutant mice was randomization of L-R asymmetry. As we have previously reported in *kif3B* null mutant mice (Nonaka et al., 1998), these null mutant mice exhibited randomized heart loop formation. Importantly, failure of cardiac looping to occur in neither direction was also encountered in *kif3A* null mutant embryos (~20%).

Then what mechanism is responsible for left-right determination? Our experiment by using fluorescent beads clearly indicated that the nodal cilia propelled certain kinds of substances in the extraembryonic fluid in the vicinity of the node from right to left. A concentration gradient that reaches the threshold for switching on *lefty* expression is probably formed and it might further destine the L-R asymmetry. This conclusion is further supported by our recent unpublished work showing randomness of left-right asymmetry occurs in mutant whose nodal pit cells harbor primary cilia, but they are immotile (Okada, Y., S. Nonaka, and N. Hirokawa, unpublished data). As a candidate of determinants, we expect that N-Shh protein might be involved since the cholesterol-conjugated form of N-Shh (Cooper et al., 1998) could not diffuse out a significant distance from a source of secretion and be concentrated to where it should be localized. There is no direct evidence for the relationship between *lefty* and *shh*, but it is now generally accepted that *shh* expression in chick is restricted to the left side before that of *lefty-2* (Levin et al., 1995). Furthermore, although the expression of *shh* is bilateral in mammals, it is most probable that the leftward flow of the extraembryonic fluid generated by nodal cilia produce the concentration gradient of secreted morphogens including Shh which are upstream of the L-R determinants such as *lefty-1*, *-2*. The absence of this flow in *kif3A* null mutant mice (Fig. 8 B) might result in disturbance of the correct topology of determinants.

As a next step in delineating the total function of KIF3 complex in vivo, conditional gene targeting is now under way. Furthermore, we could also examine the genetic interaction between these molecules by making double knockout mice for KIF3A/B. From another standpoint, by using the cell biological disciplinary, now we are also conducting experiments to unveil the function of KIF3 complex in mesodermal induction and neural development.

We should like to express our gratitude to Dr. Toshimichi Yoshida (Mie University, Japan) for the anti-axonemal outer arm dynein antibody (AD2); Dr. Winfield Sale (Emory University, Georgia) for the anti-dynein intermediate chain antibody (IC140); Dr. Hiroshi Hamada (Osaka University, Japan) for the *lefty-2* and *shh* probe; Drs. Yumiko Saga (National Institute of Health Science, Japan) and Bernhard G. Herrmann (Max-Planck Institut für Entwicklungsbiologie, Tübingen, Germany) for the *Brachyury* probe; Dr. Peter Gruss (Max-Planck Institut für Biophysikalische Chemie, Göttingen, Germany) for the *Pax6* probe. We appreciate Dr. Mika Karasawa (Chiba University, Japan) for providing us with a good protocol for whole mount in situ hybridization. We are also grateful to Drs. Yoshimitsu Kanai and Akihiro Harada, Ms. Chunjie Zhao, and Ms. Noriko Homma for their assistance in transgenic technology, and to Mrs. Haruyo Fukuda, Ms. Hiromi Sato, and Mr. Nobuhisa Ono-uchi for their technical and secretarial assistance.

This work was supported by a grant for Center of Excellence (COE) from the Ministry of Education, Science, Sports and Culture of Japan to Nobutaka Hirokawa.

Received for publication 14 January 1999 and in revised form 24 March 1999.

References

Aizawa, H., Y. Sekine, R. Takemura, Z. Zhang, M. Nangaku, and N. Hirokawa. 1992. Kinesin family in murine central nervous system. *J. Cell Biol.* 119: 1287–1296.

Beech, P.L., K. Pagh-Roehl, Y. Noda, N. Hirokawa, B. Burnside, and J.L. Rosenbaum. 1996. Localization of kinesin superfamily proteins to the con-

necting cilium of fish photoreceptors. *J. Cell Sci.* 109:889–897.
Boleti, H., E. Karsenti, and I. Vernos. 1996. Xklp2, a novel *Xenopus* centrosomal kinesin-like protein required for centrosome separation during mitosis. *Cell.* 84:49–59.
Chiang, C., Y. Litingtung, E. Lee, K.E. Young, J.L. Corden, H. Westphal, and P.A. Beachy. 1996. Cyclopia and defective axial patterning in mice lacking Sonic hedgehog gene function. *Nature.* 383:407–413.
Cole, D.G., S.W. Chinn, K.P. Wedaman, K. Hall, T. Vuong, and J.M. Scholey. 1993. Novel heterotrimeric kinesin-related protein purified from sea urchin eggs. *Nature.* 366:268–270.
Cole, D.G., D.R. Diener, A.L. Himelblau, P.L. Beech, J.C. Fuster, and I.L. Rosenbaum. 1998. *Chlamydomonas* kinesin-II–dependent intraflagellar transport (IFT): IFT particles contain proteins required for ciliary assembly in *Caenorhabditis elegans* sensory neurons. *J. Cell Biol.* 141:993–1008.
Conlon, R.A., and J. Rossant. 1992. Exogenous retinoic acid rapidly induces anterior ectopic expression of murine Hox-2 genes *in vivo*. *Development.* 116:357–368.
Conlon, F.L., C.V. Wright, and E.J. Robertson. 1995. Effects of the TWis mutation on notochord formation and mesodermal patterning. *Mech. Devel.* 49: 201–209.
Cooper, M.K., J.A. Porter, K.E. Young, and P.A. Beachy. 1998. Teratogen-mediated inhibition of target tissue response to Shh signaling. *Science.* 280: 1603–1607.
Ekker, S.C., A.R. Ungar, P. Greenstein, D.P. von Kessler, J.A. Porter, R.T. Moon, and P.A. Beachy. 1995. Patterning activities of vertebrate hedgehog proteins in the developing eye and brain. *Curr. Biol.* 55:944–955.
Fath, K.R., and D.R. Burgess. 1994. Membrane motility mediated by unconventional myosin. *Curr. Opin. Cell Biol.* 6:131–135.
Gibbons, B.H., D.J. Asai, W.J. Tang, T.S. Hays, and I.R. Gibbons. 1994. Phylogeny and expression of axonemal and cytoplasmic dynein genes in sea urchins. *Mol. Biol. Cell.* 5:57–70.
Gibbons, I.R. 1996. The role of dynein in microtubule-based motility. *Cell Struct. Func.* 21:331–342.
Grafstein, B., and D.S Forman. 1980. Intracellular transport in neurons. *Physiol. Rev.* 60:1167–1283.
Harada, A., K. Oguchi, S. Okabe, J. Kuno, S. Terada, T. Ohshima, R. Sato-Yoshitake, Y. Takei, T. Noda, and N. Hirokawa. 1994. Altered microtubule organization in small-calibre axons of mice lacking tau protein. *Nature.* 369: 488–491.
Hirokawa, N. 1996. Organelle transport along microtubules—the role of KIFs. *Trends Cell Biol.* 6:135–141.
Hirokawa, N. 1998. Kinesin and dynein superfamily proteins and the mechanism of organelle transport. *Science.* 279:519–526.
Hogan, B., R. Beddington, F. Costantini, and E. Lacy. 1994. Manipulating the Mouse Embryo: A Laboratory Manual. 2nd edition. Cold Spring Harbor Laboratory Press, Cold Spring Harbor, New York. 497 pp.
Jordan, T., I. Hanson, D. Zaletayev, S. Hodgson, J. Prosser, A. Seawright, N. Hastie, and Y. van Heyningen. 1992. The human PAX6 gene is mutated in two patients with aniridia. *Nature Genet.* 1:328–332.
Kaufman, M.H. 1995. The Atlas of Mouse Development. Academic Press, London. 525 pp.
Kondo, S., R. Sato-Yoshitake, Y. Noda, H. Aizawa, T. Nakata, Y. Matsura, and N. Hirokawa. 1994. KIF3A is a new microtubule-based anterograde motor in the nerve axon. *J. Cell Biol.* 125:1095–1107.
Kozminski, K.G., P.L. Beech, and J.L. Rosenbaum. 1995. The *Chlamydomonas* kinesin-like protein FLA10 is involved in motility associated with the flagellar membrane. *J. Cell Biol.* 131:1517–1527.
Lanske, B., A.C. Karaplis, K. Lee, A. Luz, A. Vortkamp, A. Pirro, M. Karperien, L.H.K. Defize, C. Ho, R.C. Mulligan, A.B. Abou-Samra, H. Juppner, G.V. Segre, and H.M. Kronenberg. 1996. PTH/PTHrP receptor in early development and Indian hedgehog-regulated bone growth. *Science.* 273:663–666.
Levin, M., R.L. Johnson, C.D. Stern, M. Kuehn, and C. Tabin. 1995. A molecular pathway determining left-right asymmetry in chick embryogenesis. *Cell.* 82:803–814.
Meno, C., Y. Ito, Y. Saijoh, Y. Matsuda, K. Tashiro, S. Kuhara, and H. Hamada. 1997. Two closely-related left-right asymmetrically expressed genes, *lefty-1* and *lefty-2*: their distinct expression domains, chromosomal linkage and direct neuralizing activity in *Xenopus* embryos. *Genes Cells.* 2:513–524.
Meno, C., A. Shimono, Y. Saijoh, K. Yashiro, K. Mochida, S. Ohishi, S. Noji, H. Kondoh, and H. Hamada. 1998. *lefty*-1 is required for left-right determination as a regulator of *lefty-2* and nodal. *Cell.* 94:287–297.
Mizuhira, V., and Y. Futaesaku. 1972. New fixation for biological membranes using tannic acids. *Acta Histochem. Cytochem.* 5:233–236.
Morris, R.L., and J.M. Scholey. 1997. Heterotrimeric kinesin-II is required for the assembly of motile 9+2 ciliary axonemes on sea urchin embryos. *J. Cell Biol.* 138:1009–1022.
Muresan, V., T. Abramson, A. Lyass, D. Winter, E. Porro, F. Hong, N.L. Chamberlin, and B.J. Schnapp. 1998. KIF3C and KIF3A form a novel neuronal heteromeric kinesin that associates with membrane vesicles. *Mol. Biol. Cell.* 9:637–652.
Nonaka, S., Y. Tanaka, Y. Okada, S. Takeda, A. Harada, Y. Kanai, M. Kido, and N. Hirokawa. 1998. Randomization of left-right asymmetry due to loss of nodal cilia generating leftward flow of extraembryonic fluid in mice lacking KIF3B motor protein. *Cell.* 95:829–837.
Okada, Y., H. Yamazaki, Y. Sekine-Aizawa, and N. Hirokawa. 1995. The neuron-specific kinesin superfamily protein KIF1A is a unique monomeric motor for anterograde axonal transport of synaptic vesicle precursors. *Cell.* 81: 769–780.
Rosenbaum, J.L., D.G. Cole, and D.R. Diener. 1999. Intraflagellar transport: the eyes have it. *J. Cell Biol.* 144:385–388.
Shakir, MA., T. Fukushige, H. Yasuda, J. Miwa, and S.S. Siddiqui. 1993. *C. elegans* osm-3 gene mediating osmotic avoidance behaviour encodes a kinesin-like protein. *Neuroreport.* 4:891–894.
Sulik, K., D.B. Dehart, T. Iangaki, J.L. Carson, T. Vrablic, K. Gesteland, and G.C. Schoenwolf. 1994. Morphogenesis of the murine node and notochordal plate. *Dev. Dynamics.* 201:260–278.
Supp, D.M., D.P. Witte, S.S. Potter, and M. Brueckner. 1997. Mutation of an axonemal dynein affects left-right asymmetry in inversus viscerum mice. *Nature.* 389:963–966.
Takeda, S., T. Funakoshi, and N. Hirokawa. 1995. Tubulin dynamics in neuronal axons of zebrafish embryos. *Neuron.* 14:1257–1264.
Tanaka, Y., Z. Zhang, and N. Hirokawa. 1995. Identification and molecular evolution of new dynein-like protein sequences in rat brain. *J. Cell Sci.* 108: 1883–1893.
Tanaka, Y., Y. Kanai, Y. Okada, S. Nonaka, S. Takeda, A. Harada, and N. Hirokawa. 1998. Targeted disruption of mouse conventional kinesin heavy chain, *kif5B*, results in abnormal perinuclear clustering of mitochondria. *Cell.* 93:1147–1158.
Umeda, A., T. Yoshida, K. Yamaguchi, M. Kanazawa, and C. Torikata. 1995. Immunohistochemical analysis of rat and human respiratory cilia with anti-dynein antibody: comparison between normal cilia and pathological cilia in primary ciliary dyskinesia. *Virchows Arch.* 427:401–406.
Vigh-Teichmann, I., B. Vigh, and A. Aros. 1980. Ciliated perikarya, "peptidergic" synapses and supraependymal structures in the guinea pig hypothalamus. *Acta Biol. Acad. Sci. Hunga.* 31:373–394.
Walther, Z., M. Vashishtha, and J.L. Hall. 1994. The *Chlamydomonas* FLA10 gene encodes a novel kinesin-homologous protein. *J. Cell Biol.* 126:175–188.
Wang, F.S., J.S. Wolenski, R.E. Cheney, M.S. Mooseker, and D.G. Jay. 1996. Function of myosin-V in filopodial extension of neuronal growth cones. *Science.* 273:660–663.
Willison, K. 1990. The mouse *Brachyury* gene and mesoderm formation. *Trends Genet.* 6:104–105.
Yagi, T., S. Nada, N. Watanabe, H. Tamemoto, N. Kohmura, Y. Ikawa, and S. Aizawa. 1993. A novel negative selection for homologous recombinants using diphteria toxin A fragment gene. *Anal. Biochem.* 214:77–86.
Yamazaki, H., T. Nakata, Y. Okada, and N. Hirokawa. 1995. KIF3A/B: a heterodimeric kinesin superfamily protein that works as a microtubule plus end-directed motor for membrane organelle transport. *J. Cell Biol.* 130: 1387–1399.
Yamazaki, H., T. Nakata, Y. Okada, and N. Hirokawa. 1996. Cloning and characterization of KAP3: a novel kinesin superfamily-associated protein of KIF3A/3B. *Proc. Natl. Acad. Sci. USA.* 93:8443–8448.
Yang, P., and W.S. Sale. 1998. The M_r 140,000 intermediate chian of *Chlamydomonas* flagellar inner arm dynein is a WD-repeat protein implicated in dynein arm anchoring. *Mol. Biol. Cell.* 9:3335–3339.
Yang, Z., and L.S. Goldstein. 1998. Characterization of the KIF3C neural kinesin-like motor from mouse. *Mol. Biol. Cell.* 9:249–261.
Yoshida, T., K. Katsuta, H. Takanari, and K. Izutsu. 1989. Analysis of mammalian dynein using antibodies against A polypeptides of sea urchin sperm flagellar dynein. *Exp. Cell Res.* 184:440–448.